Proceedings of the ASME 2022
International Additive Manufacturing Conference
IAM2022
October 19-20, 2022, Lisbon, Portugal

IAM2022-94060

IN-PROCESS MECHANICAL WORKING OF ADDITIVE MANUFACTURED RENE 41

William Sean James, Supriyo Ganguly, Goncalo Pardal

Welding Engineering and Laser Processing Centre, Cranfield University, UK

ABSTRACT

In developing the wire + arc additive manufacturing (WAAM) process for creep resistant alloys for defence applications, structures were built from nickel-based superalloy Rene 41 (RE41). The performance of the additive manufactured alloy was analysed for applications including components used in high-speed flight environments, where external structures could reach service temperatures of up to 1000 K. As a single use system with relatively short flight times of < 1 hour, components will be highly stressed to minimise structural mass. In this paper, three wall structures were deposited using a plasma transferred arc process, in a layer-by-layer manner where each layer was mechanically worked by machine hammer peening directly after deposition. With a constant impact frequency, three different travel speeds for the peening tool were used for each wall structure. To understand the most effective cold working parameters, samples were tested and analysed for their mechanical properties and microstructural characteristics after aging treatment. Samples were tested at room temperature and compared with results of both non-worked heat-treated AM material and wrought data obtained from literature review.

Heat-treated only material showed a typical dendritic structure with large columnar grains, and peened material showed a significantly different grain structure. No noticeable difference was observed in the formed phases between the two conditions. Mechanical testing showed promising results with a significant improvement over the non-worked strength. Intermediate and slow peening speeds were very effective, achieving UTS and YS results close to that of the wrought alloy, with a similar increase in the elastic modulus compared to non-worked material. However, faster peening speeds were less effective at returning the material to wrought strength.

NOMENCLATURE

WAAM	Wire + Arc Additive Manufacturing
DED	Directed energy deposition
RE41	Rene 41
AD	As deposited
HT	Heat-treated
RT	Room-temperature
SEM	Scanning Electron Microscope
EDS	Energy-dispersive Spectrometry
BD	Build direction
TT	Through-thickness

1. INTRODUCTION

Wire + arc additive manufacturing (WAAM) is a directed energy deposition (DED) metal AM process whereby a wire feedstock is deposited using an electrical arc as a heat source [1]. In previous studies using WAAM to deposit nickel-based superalloys, as deposited (AD) material has been unable to match the performance of the fully heat-treated (HT) wrought alloy strength, and heat-treating WAAM material does not result in a sufficient increase to match wrought strength [2]. When deposited via WAAM and tested for mechanical performance nickel-based superalloy Rene 41 (RE41), achieved just 59 % of the wrought UTS in AD condition and 61 % when the same material was HT post-deposition [3].

Highlighting the need for additional processing to meet the wrought performance, a previous study by Xu et al found that inter-pass cold rolling of WAAM Inconel 718 was able to increase the UTS of the material to where the rolled WAAM material outperformed the wrought material in both the vertical and horizontal orientations when tested [2]. In developing the WAAM process for maximising the performance of components built using RE41, a series of trials using inter-pass peening was investigated and tested to establish the most suitable peening parameters.

Large columnar grains are typically observed in WAAM built nickel-superalloy microstructure with associated segregation, which can have undesirable effects on the material properties, such as reduced strength, if large grains were not originally desired. In most cases this is due to the nickel-superalloy being precipitation strengthened or age hardened, meaning that the strength is derived mainly from the precipitation of secondary phases, such as γ', within the matrix and at the grain boundaries which inhibit dislocation motion. An elongated dendritic structure with associated segregation makes the solutionising process difficult compared to a wrought

structure where smaller grains with high angle grain boundaries facilitate the diffusion process, as such most of the wrought structures are dynamically recrystallised during rolling or other high temperature deformation processes. The large dendritic grains which make up the microstructure in WAAM material make the formation of these secondary precipitates less likely to occur as the process of diffusion is hindered due to lack of grains with large angle boundary area and segregation owing to solidification from a molten state. Xu et al also examined the effect of heat-treating WAAM built Inconel 718 and found that unless the material underwent a process to produce a more favourable microstructure the mechanical strength is unlikely to meet the wrought performance through an age hardening heat-treatment alone [4]. It should be noted that there are cases where large grains are benefitable to the performance of nickel superalloys, such as in gas turbine blades, where a single crystal is specially formed in the correct orientation to primarily improve fatigue performance [5].

RE41 shares some similarities with the strengthening mechanism of Inconel 718, however the composition varies. RE41 is a nickel-based precipitation strengthened alloy which is alloyed significantly with Cr, Co and Mo. RE41 has a face-centred-cubic austenitic matrix, and is mainly strengthened through the formation of γ' particles $Ni_3(Al,Ti)$ [6].

The benefits of WAAM over other metal AM processes such as powder bed processes, is the ability to build larger components with little adjustment or expensive equipment set-ups. WAAM is also capable of higher deposition rates when compared with power bed, which increases productivity for larger components. The metal wire feedstock used in WAAM is often less expensive than metallic powder and is easier to change for a different alloy without the need for extensive cleaning. Material loss in WAAM is also much reduced compared to powder bed which can be as much as 25 % [7]. Powder-bed does however have some advantages over WAAM, which includes the ability to create more intricate and complex lattice structures and net shape parts, whereas WAAM is a near net shape process. Parts produced using powder bed also more closely match the wrought strength of alloys [8], compared with WAAM where the need for post-processing and/or in-process working is more extensive.

The ability to manufacture larger components makes WAAM ideal for defence applications and the production of high-speed flight components. The application of such components will be in the external structure of a single use system subjected to service temperature of 1000 K for a short flight time of < 1 hour. As such components for use in this system will be highly stressed to minimise structural mass, these components will be optimised for maximum strength at maximum temperature. It is therefore the aim of this research to maximise the performance of WAAM built RE41 for this purpose.

2. MATERIALS AND METHODS

2.1 WAAM Process

A commercially available 1 mm diameter RE41 wire was used as the feedstock in a WAAM system (Figure 1) consisting of: a Kuka six-axis robotic arm, a plasma water-cooled welding torch mounted to the robotic arm, a local shielding device surrounding the plasma torch, and a wire feeder. To facilitate the inter-pass mechanical working, an Atlas Copco RRH06P riveting hammer was also mounted to the robotic arm and configured to allow for semi-automatic operation.

The composition of the RE41 wire was tested as part of a previous study using inductively coupled plasma - optical emission spectroscopy (ICP-OES), the composition is given in Table 1 [3].

A short wall approach was adopted in-order to build just enough material to extract specimens for metallographic and tensile analysis. Four walls measuring approx. 360 × 20 × 8 mm were built on an Inconel 718 substrate plate, using an arc current of 180 A, a wire feed speed of 2.4 m/min, a torch travel speed of 0.36 m/min, a torch to work distance of 8 mm, and an inter-pass temperature of 170 °C after an approx. cooling time of 3 mins. Shielding via a local shielding device, as shown in Figure 1, was provided at 30 L/min of Argon. To establish the best peening parameters one wall was built AD, without any inter-pass peening to provide a baseline. Three further walls were built using a constant impact frequency of 2160 impacts per min with a load of 30 kg, where the tool travel speed was varied for each wall. Three different travel speed of 18, 36, and 112.5 mm/s were trialled during manufacture of the walls. The use of these peening parameters provided an input energy of approx. 4.85, 2.43, 0.776 J/mm^2 for the 18, 36, and 112.5 mm/s travel speed respectively.

After the walls were manufactured, specimens for tensile, microhardness and metallographic analysis were extracted. All specimens underwent an aging heat-treatment to maximise tensile performance based on historic research by Weisenberg and Morris. The treatment consisted of: solutionising at 1065 °C for four hours followed by air quenching to room-temperature (RT) followed by a further 16 hours aging at 760 °C after which the material was again air quenched [9].

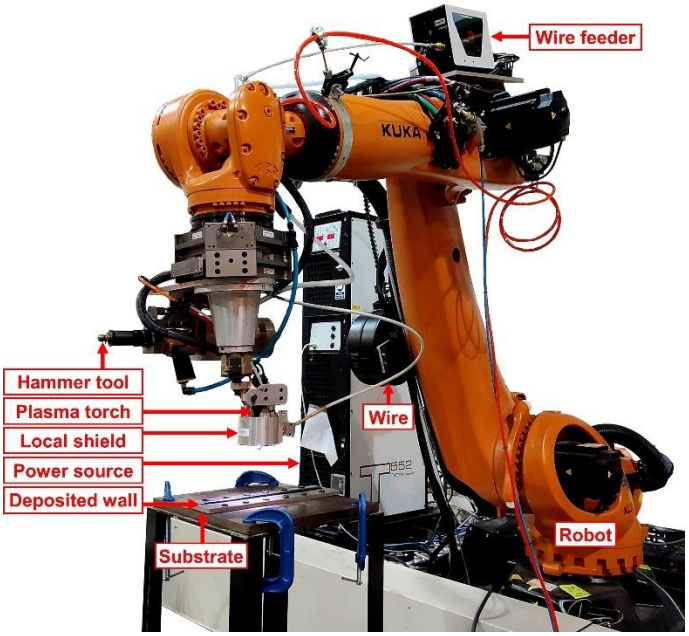

FIGURE 1: WAAM EXPERIMENTAL SETUP.

TABLE 1: COMPOSITION OF RE41 WIRE.

Ni	Cr	Co	Mo	Fe	Ti	Al	Nb	V
53.7	18.9	10.2	9.08	2.72	3.20	1.64	0.12	0.12

Si	C	Cu	Mn	B	S
0.09	0.07	0.04	0.03	0.004	<0.003

2.2 Mechanical Testing

Three tensile specimens in each condition were tested at RT to failure using an Instron 8801 Servo Hydraulic Universal Testing System. A strain rate of 0.005 mm/min was adopted until plastic deformation whereafter a rate of 1.6 mm/min was used. Testing was conducted according to the ASTM specification E8/E8M, a standard test method for tension testing of metallic materials. The specimen dimensions conformed to the sub-size category, a drawing of which is given in Figure 2.

Microhardness was measured using a Zwick/Roell hardness tester under a load of 0.5 kg and a holding time of 15 sec. Measurements were taken at 1 mm increments through the cross-section of the wall height and thickness.

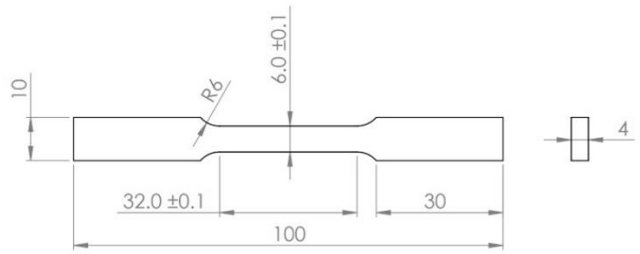

FIGURE 2: TENSILE TESTING SPECIMEN.

2.3 Metallographic Preparation and Analysis

Cross-sections in the build direction (BD) and through-thickness (TT) plane were extracted and prepared for metallographic analysis to reveal the microstructure. Following a procedure of successive grinding and polishing, samples were swab etched for 30 sec using a solution containing 3 g $CuSO_4$, 80 ml HCl, and 20 ml Ethanol.

Samples were viewed optically using a Leica DM 2700M Microscope. The microstructure was also examined using a Tescan VEGA 3 scanning electron microscope (SEM). Composition was determined by energy-dispersive spectrometry (EDS), as such the SEM was fitted with an Oxford Instruments X-Max 20 mm EDS detector.

3. RESULTS AND DISCUSSION

3.1 Mechanical

When tested at RT, tensile specimens extracted from material mechanically worked using 4.85, 2.43, and 0.776 J/mm^2, achieved an average UTS of 1284.5, 1299.4, and 1048.3 MPa and a YS of 1048.7, 1054.0, and 906.1 MPa respectively. The full set of results is presented in Table 2, where the working energies are abbreviated as W High, W Med, and W Low for 4.85, 2.43, and 0.776 J/mm^2, respectively. Figure 3 presents the stress-strain variations of material in the AD [3] and HT condition together with the worked HT material. It can be seen that with the application of higher impact energy per unit area, the elastic modulus of the material increases with the tensile strength and almost meets the performance of a wrought variant. In comparing the UTS and YS results the best performance was achieved through peening at 2.43 J/mm^2. However, when the variation in results is accounted for, it can be assumed that between the 4.85 and 2.43 J/mm^2 impacting energies, the maximum performance increase possible had been achieved by working at just 2.43 J/mm^2, due to the negligible difference in performance. Subsequently in future studies on inter-pass peening of RE41, there would be little advantage to peening beyond 2.43 J/mm^2.

In comparing the hardness of RE41 in each condition presented in Table 2, the hardness is seen to increase with impacts per area and is significantly higher that the wrought minimum. The hardness of the material affects the machinability, and difficulties were encountered during the manufacture of the tensile coupons. It is noted by Weisenberg and Morris that the rate at which RE41 work hardens makes it particularly difficult to machine, and they recommend the use of carbide tools and sulphurated oils [9]. Silicon carbide cutting disks were utilised for cutting the deposited walls from the substrate plates which worked comparatively well.

The elastic modulus (E) is also shown to vary in the results, although there is not a great deal of correlation between the working energy. Peening at room temperature hydrostatically deforms the alloy and generates dislocations and other associated metal defects which strain hardens the alloy. Subsequent transitory thermal cycles, during deposition of successive layers, would annihilate some of these dislocations but some hardening

effects will remain which would work to make the deposit stiffer when compared to the non-worked variant. It should also be noted this difference could be due to E being calculated from tensile data which can be error prone. Further investigation is required to fully discuss this observation.

TABLE 2: MECHANICAL PERFORMANCE AT RT.

Condition	UTS (MPa)	YS (MPa)	E (GPa)	HV
Wrought [10]	1420	1060	220	363 (min)
HT	880.8	829.4	161.4	406.3
HT + W Low	1048.3	906.1	156.7	437.2
HT + W Med	1299.4	1054.0	194.4	442.9
HT + W High	1284.5	1048.7	186.3	459.0

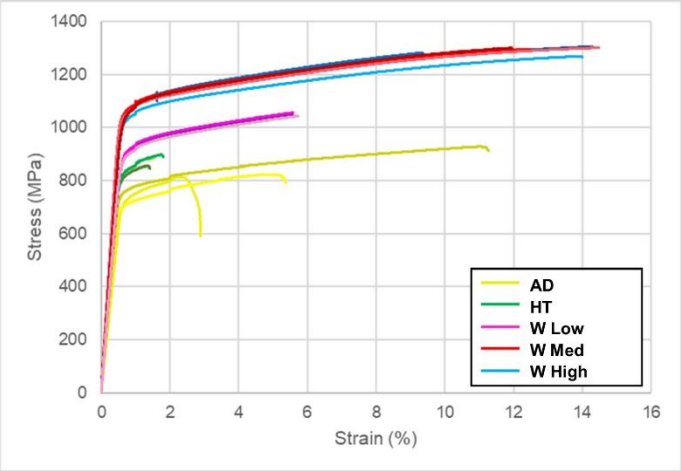

FIGURE 3: STRESS-STRAIN OF RT MECHANICAL PERFORMANCE.

3.2 Microstructural Observations

Of the examined specimens there is observable differences in the macrostructure of the HT and worked material, seen in Figure 4. The main differences are in the granular structure, where the dendritic structure of the worked material has been disrupted by the peening process, leading to the disruption of the long columnar grain structure which is so typically observed in alloys deposited via wire-arc DED processes. This affect is best observed when comparing HT material in Figure 5 and the worked material Figure 6.

No cracking was observed in worked material; however, several large solidification cracks were observed in the HT material (Figure 4), note that of these cracks only the largest is visible in Figure 4. Solidification cracks were identified based on orientation along the BD axis owing to lateral stresses and segregation at the crack edge. The crack edge segregation can be seen in Figure 7. It is thought that the stress input into the material due to peening has allowed for relaxation of the strain created during the deposition process, which has subsequently resulted in the elimination of cracking. Cracking has been known to occur in DED built superalloys, notably in WAAM built Inconel 718 [11]. Atabay et al found that RE41 did not experience cracking when used in laser powder bed fusion (LPBF), and attributed this to the fine microstructure produced when using LPBF [12], it is possible that the disruption of the typically larger grain structure seen in WAAM components has resulted in the both an increased strength and a reduction in susceptibility to cracking.

When the microstructure is examined at greater magnification using a SEM the difference between HT only (Figure 8) and worked material (Figure 9) is negligible, with the same phases observed in both specimens, indicating that the in-process working has no impact on the formed phases. An EDS mapping (Figure 10) and composition table (Table 3) is provided for the phases observed in the worked material. Lighter coloured areas are indicative of Mo rich phases, likely a complex intermetallic known as σ phase (CrNiMo) which is known to occur in nickel superalloys [13], these phases were analysed using EDS and the results are presented in Table 3. The darker grey coloured phases however are indicative of Ti rich precipitates, suggesting the presents of Ti rich carbides.

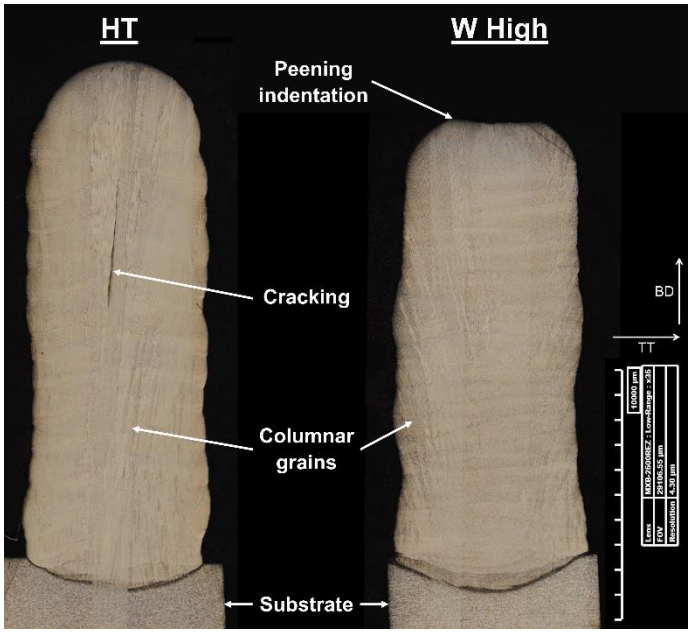

FIGURE 4: MACROSRUCTURE OF HT AND WORKED (W HIGH) MATERIAL.

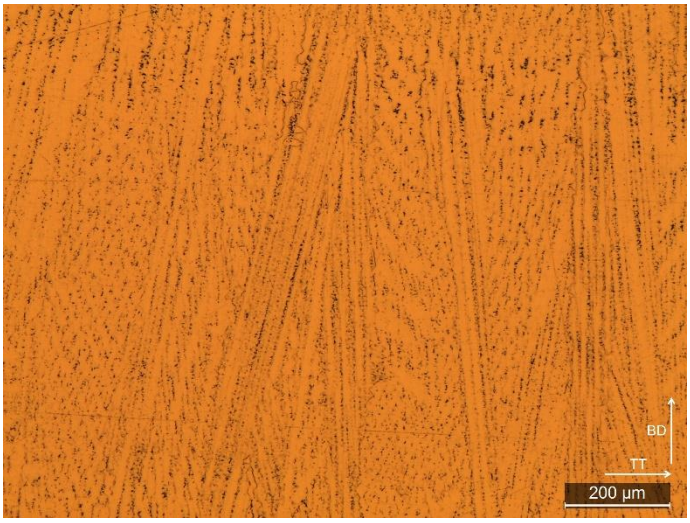

FIGURE 5: MICROGRAPH OF HT MATERIAL DISPLAYING LONG COLUMNAR GRAIN STRUCTURE.

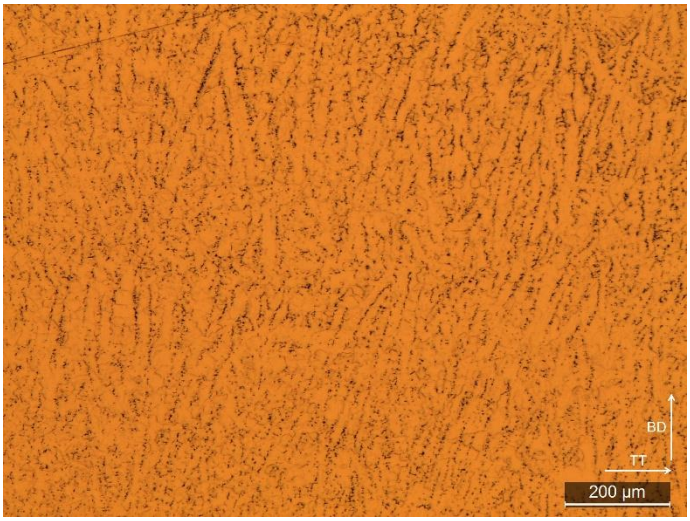

FIGURE 6: MICROGRAPH OF WORKED (W HIGH) SHOWING DISTRUPTED DENDRITIC STRUCTURE.

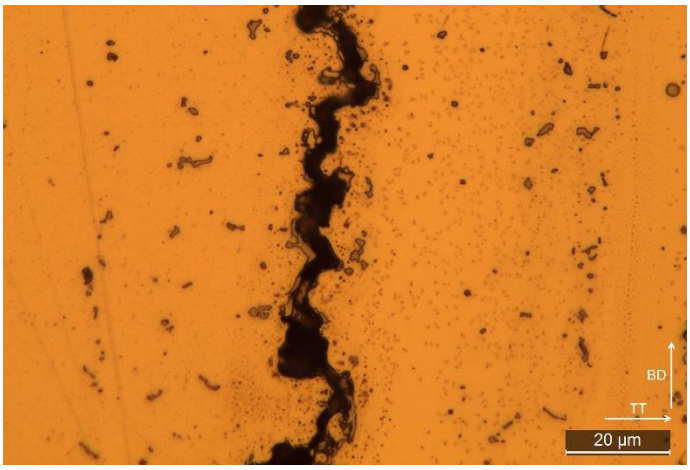

FIGURE 7: SOLIDIFICATION CRACK OBSERVED IN HT SAMPLE SEEN IN FIGURE 4.

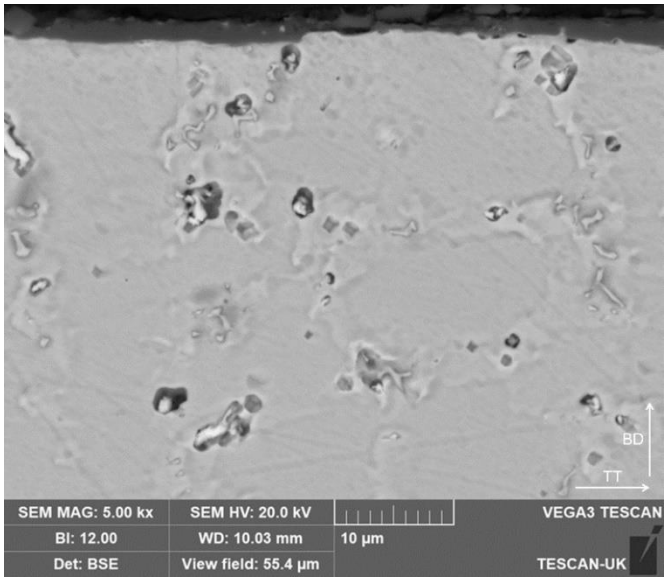

FIGURE 8: SEM BSE IMAGE OF HT MATERIAL.

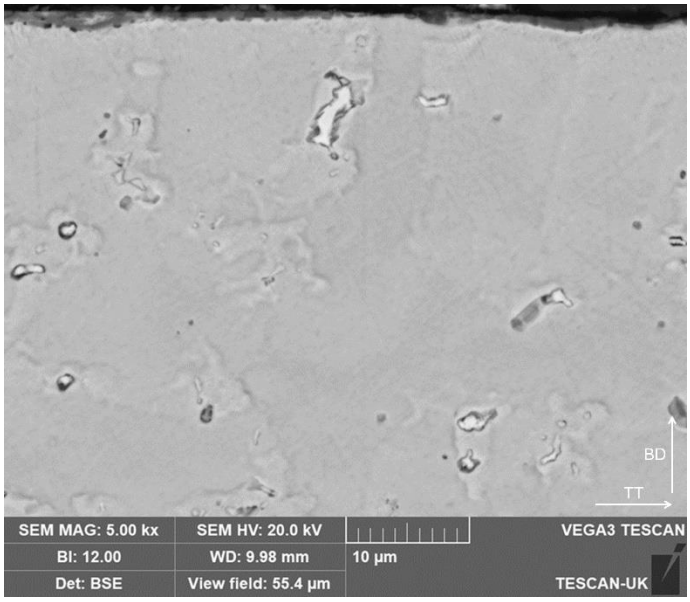

FIGURE 9: SEM BSE IMAGE OF WORKED (W HIGH) MATERIAL.

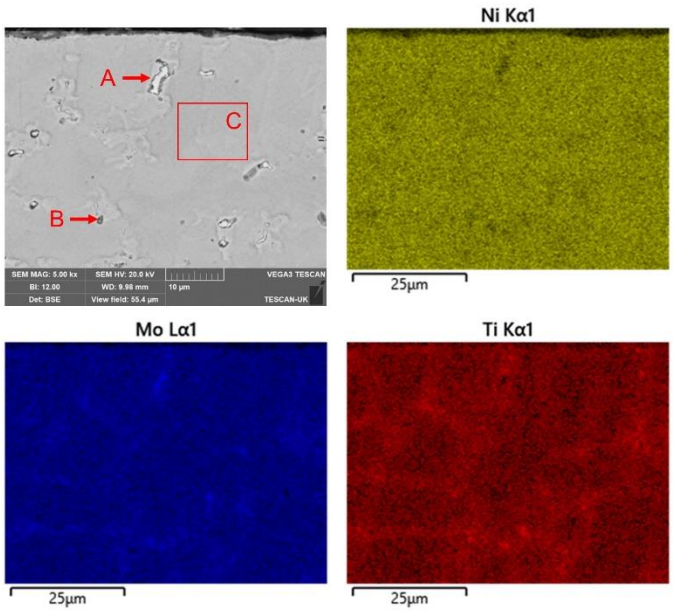

FIGURE 10: EDS ELEMENTAL MAPPING OF WORKED (W HIGH) MATERIAL.

TABLE 3: EDS COMPOSITION OF AREAS MARKED IN FIGURE 10 (% AT.).

Element	Spectrum A	Spectrum B	Spectrum C
Al	1.48	2.37	3.72
Ti	3.35	12.24	3.22
V	0.15		0.12
Cr	31.40	20.08	21.39
Fe	2.35	2.51	3.00
Co	9.70	8.94	10.44
Ni	30.73	46.64	52.67
Mo	20.84	7.22	5.44

4. CONCLUSION

- In-process working during WAAM deposition can increase the performance of RE41 by up to 48 % over HT only material.
- Use of a peening energy density of more than 2.43 J/mm^2 does not result in any additional benefit.
- RE41 work hardens quickly, and microhardness increases with work done.
- In-process working of RE41 disrupts the long columnar grain structure typically observed in wire-arc DED built material.
- In-process working of RE41 results in a decreased susceptibility to cracking.

ACKNOWLEDGEMENTS

The authors wish to acknowledge the Ministry of Defence (UK) for their financial support, and the industrial supervisors from DSTL Porton Down, for their ongoing advice and guidance: Graham Simpson and Dr Matthew Lunt.

REFERENCES

[1] S. W. Williams, F. Martina, A. C. Addison, J. Ding, G. Pardal, and P. Colegrove, “Wire + Arc additive manufacturing,” *Mater. Sci. Technol.*, vol. 32, no. 7, pp. 641–647, 2016.

[2] X. Xu, S. Ganguly, J. Ding, C. E. Seow, and S. Williams, “Enhancing mechanical properties of wire + arc additively manufactured INCONEL 718 superalloy through in-process thermomechanical processing,” *Mater. Des.*, vol. 160, pp. 1042–1051, 2018.

[3] W. S. James, S. Ganguly, and G. Pardal, “[Manuscript submitted for publication] High Temperature Failure and Microstructural Investigation of Additive Manufactured Rene 41,” *Mater. Sci. Eng. A*, 2022.

[4] X. Xu, J. Ding, S. Ganguly, and S. Williams, “Investigation of process factors affecting mechanical properties of INCONEL 718 superalloy in wire + arc additive manufacture process,” *J. Mater. Process. Technol.*, vol. 265, no. September 2018, pp. 201–209, 2019.

[5] N. K. Arakere and G. Swanson, “Effect of crystal orientation on fatigue failure of single crystal nickel base turbine blade superalloys,” *J. Eng. Gas Turbines Power*, vol. 124, no. 1, pp. 161–176, 2002.

[6] M. Schwartz, R. Ciocoiu, D. Gheorghe, G. Jula, and I. Ciucă, “Preliminary research for using Rene 41 in confectioning extrusion dies,” *Mater. Characterisation VII*, vol. 1, pp. 95–106, 2015.

[7] A. N. M. Tanvir *et al.*, “Heat treatment effects on Inconel 625 components fabricated by wire + arc additively manufacturing (WAAM)—part 2: mechanical properties,” *Int. J. Adv. Manuf. Technol.*, vol. 110, no. 7–8, pp. 1709–1721, 2020.

[8] X. Wang, X. Gong, and K. Chou, “Review on powder-bed laser additive manufacturing of Inconel 718 parts,” *Proc. Inst. Mech. Eng. Part B J. Eng. Manuf.*, vol. 231, no. 11, pp. 1890–1903, 2017.

[9] L. A. Weisenberg and R. J. Morris, “How to Fabricate Rene 41,” *Met. Prog.*, vol. 78, pp. 70–74, 1960.

[10] M. J. Donachie and S. J. Donachie, “Selection of Superalloys,” in *Superalloys - A Technical Guide*, 2nd ed., ASM International, 2002, pp. 11–24.

[11] W. S. James, S. Ganguly, and G. Pardal, “[Manuscript submitted for publication] Microstructure and Mechanical Properties of Inconel 718 and Inconel 625 Produced Through the Wire + Arc Additive Manufacturing Process,” in *AVT-356 Physics of Failure for Military Platform Critical Subsystems*, 2021.

[12] S. E. Atabay, O. Sanchez-Mata, J. A. Muñiz-Lerma, R. Gauvin, and M. Brochu, “Microstructure and mechanical properties of rene 41 alloy manufactured by laser powder bed fusion,” *Mater. Sci. Eng. A*, vol. 773, no. October 2019, 2020.

[13] H. E. Collins, “Relative Stability of Carbide and Intermetallic Phases in Nickel-Base Superalloys,” in *International Symposium on Structural Stability in Superalloys*, 1968, pp. 171–198.